analytical chemistry

Article

pubs.acs.org/ac

Bacterial Pathogen Surface Plasmon Resonance Biosensor Advanced by Long Range Surface Plasmons and Magnetic Nanoparticle Assays

Yi Wang,[†,‡] Wolfgang Knoll,[†,‡] and Jakub Dostalek*[,†]

[†]Austrian Institute of Technology, Muthgasse 11/2, 1190 Vienna, Austria

[‡]Nanyang Technological University, Centre for Biomimetic Sensor Science, Singapore 637553

Supporting Information

ABSTRACT: A new approach to surface plasmon resonance (SPR) biosensors for rapid and highly sensitive detection of bacterial pathogens is reported. It is based on the spectroscopy of grating-coupled long-range surface plasmons (LRSPs) combined with magnetic nanoparticle (MNP) assay. The interrogation of LRSPs allows increasing the biosensor figure of merit (FOM), and the employment of MNPs further enhances the sensor response by a fast delivery of the analyte to the sensor surface and through the amplified refractive index changes associated with the capture of target analyte. This amplification strategy is particularly attractive for detection of large analytes that diffuse slowly from the analyzed sample to the sensor surface. The potential of the presented approach is demonstrated in a model experiment in which *Escherichia coli* O157:H7 was detected at concentrations as low as 50 cfu mL^{-1}, 4 orders of magnitude better than the limit of detection achieved by regular grating-coupled SPR with direct detection format.

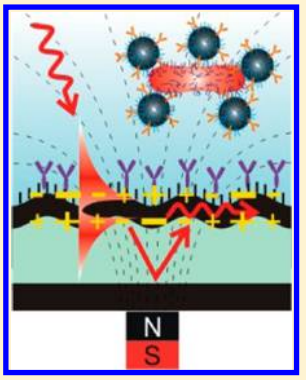

Surface plasmon resonance (SPR) biosensors represent rapidly advancing technology for fast and sensitive detection of chemical and biological analytes in important applications areas of medical diagnostics, food control, and environmental monitoring.[1] SPR offers the advantage of direct label-free detection method that relies on the measurement of refractive index changes accompanied with the binding of target analyte. The specific capture of target analyte on metallic sensor surface with attached biomolecular recognition elements is probed by resonantly excited surface plasmons. These modes originate from coupled oscillations of charge density and the associated electromagnetic field occurring at a distance up to approximately hundred nanometers from the metal. Over the last years, we witnessed extensive research efforts aimed at the implementation of SPR biosensors for rapid detection of bacterial pathogens.[2−5] However, they were typically shown to allow for the analysis of bacterial pathogens at concentrations above 10^3 colony forming units (cfu) per mL which is not sufficient for the majority of harmful pathogens. The key limitations impeding the sensitivity of bacterial pathogen SPR biosensors are related to small refractive index contrast of the analyte bound to the surface, slow diffusion-driven mass transfer from a sample to the sensor surface, and insufficient depth probed by surface plasmons which is much smaller than the micrometer characteristic size of bacteria.

Numerous amplification strategies were pursued for advancing SPR biosensors based enzymatic reactions,[6] metallic[7,8] and magnetic[9−14] nanoparticle assays, as well as by combining SPR with fluorescence spectroscopy.[15] Parallel to amplification strategies, improving the sensitivity through increasing the accuracy of refractive index measurements was subject to research in SPR sensors utilizing propagating and localized surface plasmons on nanostructured metallic surfaces.[16,17] Among these, the employing of long-range surface plasmons (LRSPs), which propagate along thin metal films embedded in a refractive index symmetrical layer architecture,[18] were investigated for high-resolution SPR biosensors.[19] LRSP modes exhibit lower losses compared to regular surface plasmons, which translates into narrower resonance. Therefore, they allow for improving the figure of merit (FOM)[19,20] and more accurate measurement of refractive index variations. In addition, the profile of LRSP field can be tuned to probe an order of magnitude higher distances from the metal surface compared to regular surface plasmons,[20] which makes them excellently suited for the analysis of large analytes such as bacterial pathogens.[21,22]

This paper describes a new approach to SPR biosensors for the detection of bacterial pathogens that utilizes nanostructured surface architecture comprising low refractive index fluoropolymer and metallic layers for the diffraction grating-based excitation and interrogation of LRSPs. The developed sensor chip enables straightforward implementation of amplification strategies relying on magnetic nanoparticle (MNP) assays. This approach is employed for the rapid delivery of target analyte from a sample to the sensor surface by a magnetic field gradient that is applied through the sensor chip. Let us note that this feature is particularly advantageous for detection of large analytes and its implementation to more commonly used prism-based SPR biosensors is not possible. The performance characteristics of the developed sensor platform are shown by

Received: July 9, 2012
Accepted: August 29, 2012
Published: August 29, 2012

   dx.doi.org/10.1021/ac301904x | *Anal. Chem.* 2012, 84, 8345−8350

using an immunoassay experiment for the detection of *Escherichia coli* O157:H7, and the achieved results are compared to those that were determined in an identical experiment by regular diffraction grating-coupled SPR.

MATERIALS AND METHODS

Materials. Magnetic iron oxide nanoparticles modified with a polysaccharide layer (fluidMAG-ARA with diameter of ~200 nm, magnetic core diameter of ~175 nm) were purchased from Chemicell (Berlin, Germany). *E. coli* O157:H7 standard was obtained from KPL Inc. (Gaithersburg, MD), and *E. coli* strain K12 was cultivated in our laboratory. The average diameters of heat-killed *E. coli* O157:H7 and K12 were determined by dynamic light scattering (DLS) with Zetasizer from Malvern Instruments (Worcestershire, U.K.) as 1177 and 869 nm, respectively. Capture antibody against *E. coli* O157:H7 (cAb, no. ab75244) was from Abcam (Cambridge, U.K.). Affinity-purified detection antibody against *E. coli* O157:H7 (dAb, no. 01-95-90) was obtained from KPL (Gaithersburg, MD). 1-Ethyl-3-(3-dimethylaminopropyl)carbodiimide (EDC) and *N*-hydroxysuccinimide (NHS) were from Pierce (Rockford). Dithiolaromatic PEG6-carboxylate (thiol-COOH) and dithiolaromatic PEG3 (thiol-PEG) were from SensoPath Technologies (Bozeman, MT). 2-(*N*-Morpholino)ethanesulfonic acid (MES), phosphate buffered saline (PBS) tablets, and Tween-20 were acquired from Sigma-Aldrich (Austria). All detection experiments were carried out in PBS buffer with 0.05% Tween 20 (PBST). Low-refractive index polymer, Cytop CTL-809 M, and UV-curable polymer NOA 72 were obtained from Asahi Inc. (Japan) and Norland (Cranbury, NJ), respectively. Polydimethylsiloxane (PDMS) and its curing agent SYLGARD 184 were from Dow Corning.

Preparation of Sensor Chip. Nanostructured layer architectures for the diffraction grating-based excitation of long-range surface plasmons and regular surface plasmons were prepared by a variant of nanoimprint lithography (NIL). First, a silicon master with sinusoidal relief modulation (period of Λ = 510 nm and modulation depth of d = 27 nm) was fabricated by interference lithography and reactive ion beam etching. Afterward, the corrugated surface of the silicon master was casted to a PDMS stamp which was used to transfer the corrugation onto used sensor chips, see Figure 1a. For the grating-coupled long-range surface plasmon (GC-LRSP) sensor chips, a 100 nm gold film was first deposited on a flat glass substrate by sputtering (UNIVEX 450C from Leybold Systems, Hanau, Germany) followed by the spin-coating of a low-refractive index fluoropolymer film. The Cytop fluoropolymer was used as it exhibits a refractive index of n_b = 1.338 (at the wavelength λ = 633 nm) that is close to that of water n_s = 1.332 and its structuring by using nanoimprint lithography was reported by other groups previously.[23] The Cytop layer was deposited with the thickness of d_b = 630 nm followed by the attachment of the PDMS stamp to its top after a 5-min predrying. The surface contacted with PDMS stamp was completely dried overnight in vacuum oven at 50 °C, the PDMS stamp was detached, and a gold layer with the thickness of d_m = 25 nm was sputtered on the corrugated Cytop surface. The gold grating on GC-LRSP chip exhibited the same period Λ = 510 nm as the master and a decreased modulation depth of 12 nm as was determined by atomic force microscopy (AFM). For the reference sensor chip with regular grating-coupled surface plasmon (GC-SP) resonance, the silicon master corrugation was transferred to a UV-curable polymer NOA72 that was subsequently coated by a 60 nm thick gold layer as described in our previous work.[13] The GC-SP sensor chip carried a gold grating with the period Λ = 510 nm and a deeper modulation depth d = 27 nm.

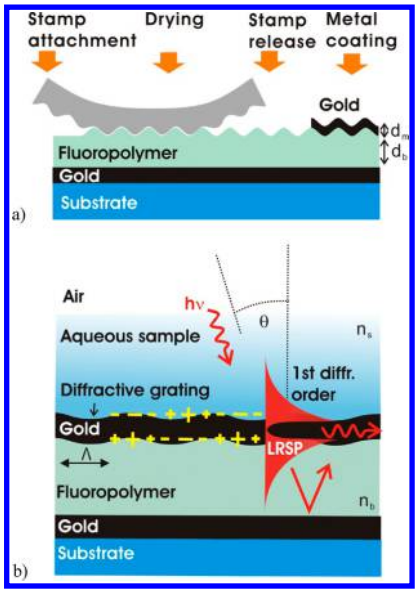

Figure 1. (a) Preparation of the layer structure supporting GC-LRSP with an imprinting of a relief corrugation to a low-refractive index Cytop fluoropolymer layer. (b) Schematic of the sensor chip for the optical excitation of and interrogation of GC-LRSPs.

Thiol self-assembled monolayer (SAM) was formed on the gold surface of GC-SP and GC-LRSP chips by the overnight incubating in a mixture of thiol-COOH and thiol-PEG dissolved at a molar ratio of 1:9 in absolute ethanol (total concentration of 1 mM). On the mixed thiol SAM, cAb was covalently bound via the amine groups after the activation of SAM carboxyl groups by a mixture of EDC (37.5 mg mL^{-1}) and NHS (10.5 mg mL^{-1}).

Optical Setup. An optical setup for angular spectroscopy of surface plasmon modes shown in Figure 2a was used. This setup was derived from that previously employed in our laboratory.[13] Briefly, a light beam with the wavelength of λ = 632.8 nm from a He−Ne laser (Uniphase, CA) was made incident at a surface of a GC-LRSP or regular GC-SP sensor chip. The sensor chip was mounted on a rotation stage (Huber AG, Germany) in order to control the angle of incidence θ. The intensity of the laser beam that was reflected from the sensor chip surface was measured by using a photodiode (PD) connected to a lock-in amplifier (Princeton Applied Research, TN). A flow-cell with the volume of about 10 μL was clamped to the surface of the sensor chip. Samples were flowed over the sensor surface at a flow-rate of 503 μL min^{-1}. This setup allowed for the measurements of angular reflectivity spectra $R(\theta)$ as well as the kinetics of the reflectivity signal at an angle θ set at the highest slope of the GC-LRSP or GC-SP resonance dip. For the MNP-enhanced assays, an external magnetic field with a gradient perpendicular to the surface of ∇B = 0.10 T mm^{-1} was applied by using a 1.4T NdFeB cylindrical magnet from Neotexx (Berlin, Germany) that was placed at the distance of 2 mm from the sensor surface. The magnet diameter and length were of 10 and 25 mm, respectively.

Modification of MNPs with dAb. MNPs were decorated with dAb against *E. coli* O157:H7 (see Figure 2b) according to the protocol provided by the supplier with several modifica-

dx.doi.org/10.1021/ac301904x | *Anal. Chem.* 2012, 84, 8345−8350

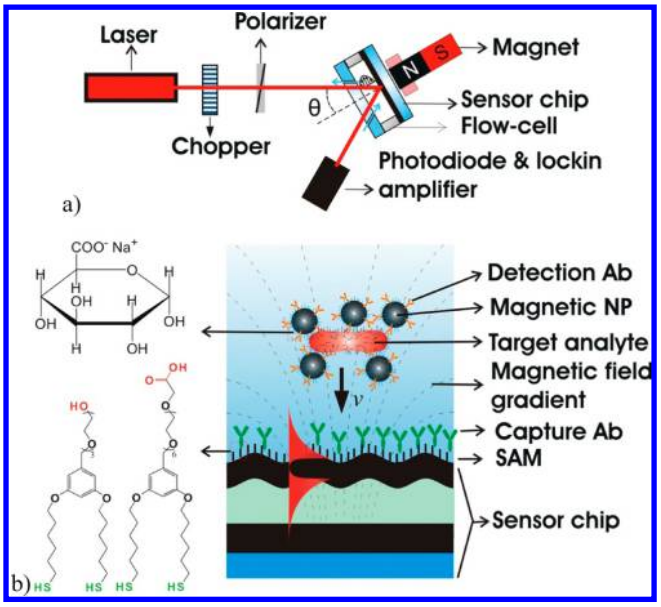

Figure 2. (a) Optical setup utilizing GC-LRSPs and (b) used surface architecture for the detection of bacterial pathogens by MNP-enhanced assay.

tions. Briefly, 20 mg of MNPs-ARA were activated in 2-(*N*-morpholino)ethanesulfonic acid (MES) buffer with EDC and NHS dissolved at a concentration of 11 mg mL^{-1}. Afterward, MNPs were washed with pure MES buffer and incubated with 100 μg of dAb for 2 h at room temperature. Then, the MNPs-dAb conjugates were deactivated by the reaction with 1 M ethanolamine (pH 8.5) for 20 min followed by the washing with PBST. The antibody-to-MNP ratio was estimated as 10:1, assuming 90% of antibodies were immobilized on the MNPs surface during the labeling process.[24]

Detection Formats. All samples were prepared by spiking PBST with target *E. coli* O157:H7 or reference *E. coli* K12 analytes at concentrations between 10^3 and 10^7 cfu mL^{-1}. In direct detection format, the samples were flowed over the sensor surface with immobilized cAbs for 15 min followed by the rinsing with PBST. In the MNPs-enhanced assay, MNPs conjugated with dAb were mixed with a sample containing target analyte *E. coli* O157:H7 or control analyte *E. coli* K12 and incubated for 15 min. Afterward, the mixture was circulated through the sensor for 10 min with the magnetic field gradient of ∇B = 0.10 T mm^{-1} applied through the sensor chip. Then, the surface was rinsed for 1 min with PBST, the magnet was removed from the sensor surface leading to ∇B = 0, and the surface was rinsed for additional 5 min. In order to use the sensor chip for multiple experiments, 10 mM NaOH was flowed over the sensor surface for several minutes to release the captured analyte and leave the unoccupied cAb binding sites available for the next detection cycle. Let us note that dAb conjugated to MNPs is specific to analyte epitopes different from that for cAb.

RESULTS AND DISCUSSION

Sensitivity of GC-SP and GC-LRSP Sensor Chips. Grating structures for the excitation of regular surface plasmons (GC-SP) and long-range surface plasmons (GC-LRSP) were designed for the first diffraction order coupling of an optical wave incident at the surface. The diffraction on the periodically modulated gold surface allows one to enhance the parallel component of the light beam propagation constant $2\pi/\lambda \sin(\theta)$ by the grating momentum $2\pi/\Lambda$ to match that of SP or LRSP. On the GC-LRSP sensor chip, the light beam is partially reflected and partially transmitted through the corrugated gold film which hinders the coupling strength to LRSPs. In order to increase the coupling efficiency, an additional flat metal film between the fluoropolymer buffer layer and the glass substrate was used. This layer reflects the transmitted beam back toward to LRSP-guiding gold layer and prevents the leaking of LRSPs into the substrate, see Figure 1b. The thickness of the fluoropolymer layer of d_b = 633 nm was adjusted to provide constructive interference between the (normal) incident and back-reflected beams at the corrugated gold surface. Simulations based on the finite element method (FEM) were carried out in order to optimize the design of the prepared structure as described in the Supporting Information (Figure S1).

As Figure 3a shows, the grating coupling to long-range surface plasmons (GC-LRSP) and regular surface plasmons

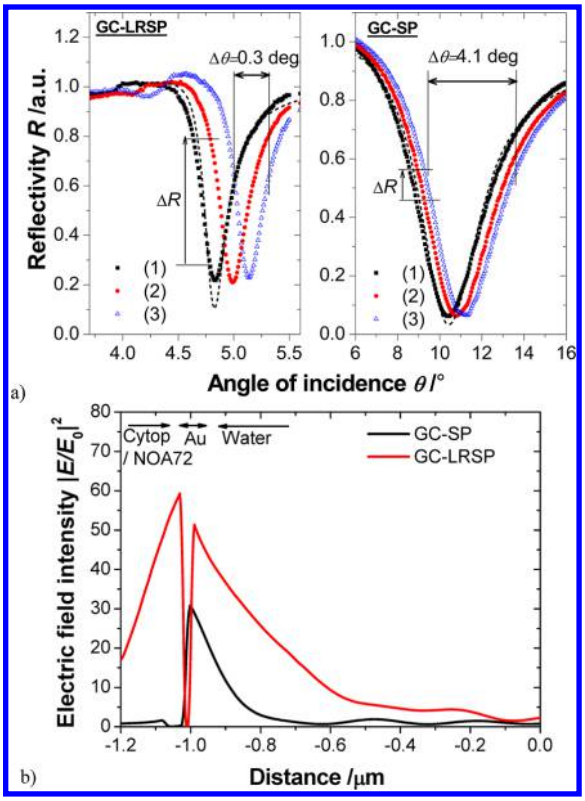

Figure 3. (a) Measured angular reflectivity spectra from GC-LRSP and GC-SP sensor chips brought in contact with a series of aqueous samples spiked with ethylenglycol. Refractive indices of samples were (1) n_s = 1.3326, (2) n_s = 1.3330, and (3) n_s = 1.3334. Dashed lines represent simulated reflectivity. (b) Simulated profile of electric field intensity perpendicular to the sensor surface upon the resonant coupling to GC-SPs (black curve) and LRSPs (red curve).

(GC-SP) manifests itself as a narrow dip in the reflectivity spectrum centered at an angle θ where the incident and plasmon waves are diffraction phase-matched. GC-SP resonance occurs at an angle (θ = 10°) that is higher than the one where the GC-LRSP excitation occurs (θ = 5°) due to higher momentum of SPs. If the refractive index of a sample on the gold surface n_s is increased, the resonance dips shift to higher angles θ. The angular sensitivity to refractive index changes defined as $S = \delta\theta/\delta n_s$ is lower for GC-LRSP (S = 38° RIU^{-1})

dx.doi.org/10.1021/ac301904x | *Anal. Chem.* 2012, 84, 8345−8350

than that for regular GC-SP (S = 92° RIU^{-1}). The reason is that LRSP field propagates on both sides of the thin corrugated metallic film, while that of regular SP is fully confined in the sample, see Figure 3b. However, the figure of merit (FOM, defined as the ratio of the angular sensitivity S and width of the resonance $\Delta\theta$) is about 5 times better for GC-LRSP (FOM = 127) compared to that for GC-SP (FOM = 24) as the coupling to LRSPs is associated with a narrower resonance. This leads to increased changes in the reflectivity R due to refractive index changes δn_s at an angle fixed at the highest slope of the resonance dip (θ = 4.77° for GC-LRSP and θ = 9.85° for GC-SP). The sensitivity of the reflectivity changes ΔR to refractive index variations δn_s was enhanced by a factor of 8.5 (see Figure S2 in Supporting Information) which is better than that predicted by the FOM, and it is caused by the nonsymmetrical shape of the resonant dip. The electric field intensity distribution $|E/E_0|^2$ was calculated by using FEM for the resonant coupling to LRSPs and regular SPs (see respective simulated reflectivity curves in Figure 3a). Results in Figure 3b predict that LRSP probes to a 3-fold higher distance from the metal surface than regular surface plasmons. Therefore, the combined higher probing depth and increased refractive index sensitivity makes GC-LRSP a better suited platform than regular GC-SP for the detection of specifically captured large bacterial pathogens on the sensor surface that is functionalized with cAb.

Magnetic Nanoparticle-Enhanced Immunoassay for *E. coli* O157:H7. First, the angular reflectivity spectra were measured from GC-LRSP and GC-SP sensor chips before and after the affinity capture of *E. coli* O157:H7 analyte that was reacted with MNP-dAb and pulled to the sensor surface by applied magnetic field gradient ∇B. As Figure 4a shows, the GC-SP and GC-LRSP resonances shift to higher angles as increasing the concentration of *E. coli* O157:H7 in the sample, indicating the binding of *E. coli* O157:H7 to cAb. In addition, the overall reflectivity decreases for higher analyte concentrations due to the strong scattering and absorption of MNP aggregates on the sensor surface. In further detection experiments, the maximum reflectivity changes ΔR were measured at the angle of incidence of θ = 5° for GC-LRSP and θ = 11.5° for GC-SP. These changes were determined as the difference in the reflectivity signal R before the injection of a sample and after the rinsing with PBST. From Figure 4a follows that the capture of target analyte on the sensor surface is accompanied with a significantly higher reflectivity change ΔR on GC-LRSP sensor chip than on that supporting regular GC-SPs. The enhancement of the reflectivity change (defined as the ratio of ΔR for GC-LRSP and GC-SP) is increasing when decreasing the analyte concentration, and values of 2.4 and 4 were obtained for the concentrations 10^7 cfu mL^{-1} and 10^3 cfu mL^{-1}, respectively. These factors are lower than those observed in previous refractometric experiments (factor of 8.5), which is probably due to the effect of absorption changes. In addition, the dependence of the enhancement factor on the *E. coli* O157:H7 concentration indicate that the density distribution of MNP perpendicular to the surface plays an important role for probing the sensor surface to different depths by LRSPs and regular SPs (see Figure 3b) .

In order to maximize the enhancement of the sensor response ΔR by MNP-assisted pulling of target *E. coli* O157:H7 analyte to the surface, the concentration of MNPs conjugated with dAb and preincubated with a sample was optimized. The sensor response ΔR was measured by using GC-SPs for the

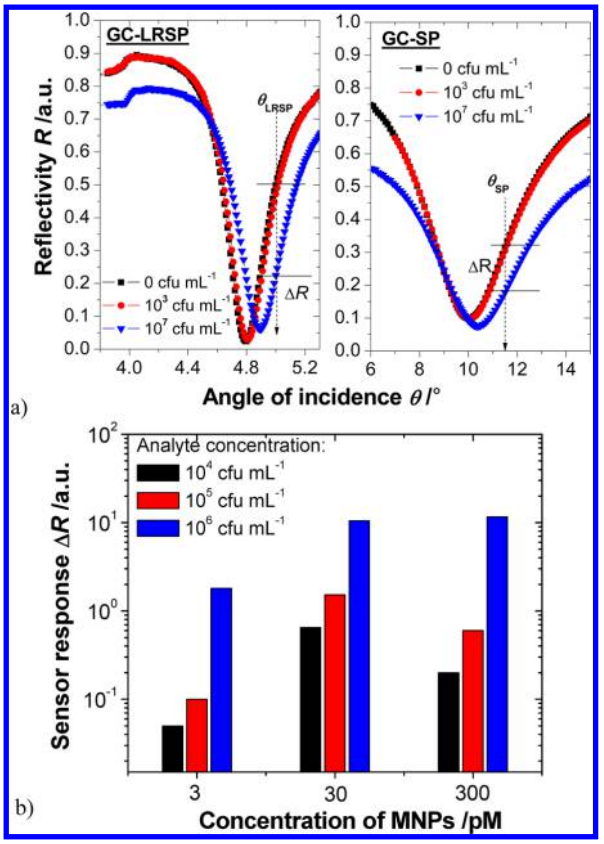

Figure 4. (a) A comparison of angular reflectivity spectra measured after the capture of *E. coli* O157:H7 at concentrations of 0, 10^3, 10^7 cfu mL^{-1} on GC-SP and GC-LRSP sensor chips (MNP-dAb concentration was 30 pM). (b) Reflectivity changes measured by GC-SP resonance after the affinity capture of *E. coli* O157:H7 dissolved at concentrations of 10^4, 10^5, and 10^6 cfu mL^{-1} and incubated with MNP-dAb conjugates at concentrations of 3, 30, and 300 pM.

MNP-dAb concentrations of 3, 30, and 300 pM and analyte concentrations of 10^4, 10^5, and 10^6 cfu mL^{-1}. The results presented in Figure 4b indicate that the MNP-dAb concentration providing maximum sensor response decreases with decreasing the concentration of target analyte. The reason for this observation is that the magnetic field gradient ∇B pulls to the sensor surface both MNPs bound to the analyte and those not reacted with the analyte. Therefore, a balance between the efficient analyte delivery to the surface and avoiding blocking of cAb active sites by the excess of free MNP-dAb which does not contribute to the sensor response needs to be established. In further experiments, the concentration of MNP-dAb was fixed at 30 pM, which provided the highest sensor response for the concentration of analyte around 10^4 cfu mL^{-1}.

Performance Characteristics. The sensor response to the binding of target analyte *E. coli* O157:H7 was compared for the direct detection format on a regular GC-SP sensor chip with that for the MNP-enhanced assay combined with the readout based on GC-LRSP. The measured reflectivity kinetics for the direct GC-SP assay is presented in Figure 5a (measured at the angle of incidence θ = 9°). It shows a gradual increase in the reflectivity signal R upon the binding of *E. coli* O157:H7 to the surface and reveals that the reflectivity change ΔR increases with the analyte concentration. For instance, the reflectivity change reached $\Delta R = 1.2 \times 10^{-3}$ for the *E. coli* O157:H7 concentration of 10^6 cfu mL^{-1}. For the MNP-enhanced assay performed on the GC-LRSP sensor chip that is shown in Figure

dx.doi.org/10.1021/ac301904x | *Anal. Chem.* 2012, 84, 8345−8350

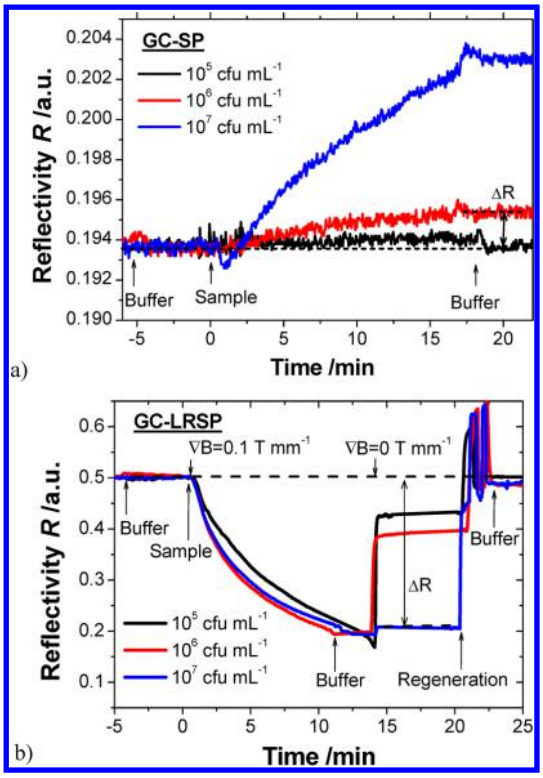

Figure 5. Kinetics of reflectivity signal for (a) direct detection assay with probing of *E. coli* O157:H7 binding by GC-SPs and (b) MNPs immunoassay-enhanced assay with probing by GC-LRSPs.

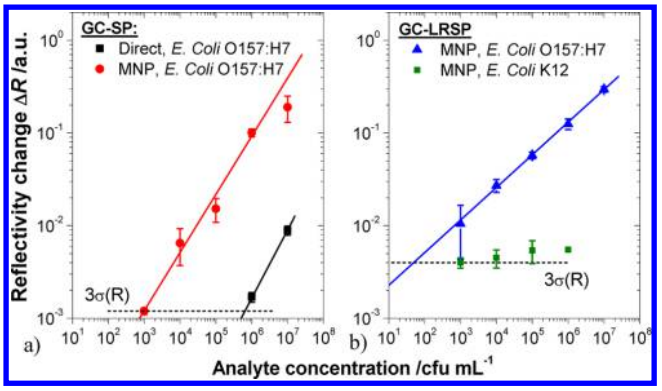

Figure 6. Calibration curves for (a) GC-SP with direct and MNP-enhanced detection of target *E. coli* O157:H7 and (b) for GC-LRSP combined MNPs-enhanced assay for detection of target analyte *E. coli* O157:H7 and a control analyte *E. coli* K12.

5b, the reflectivity signal gradually decreases after the injection of a sample preincubated with MNP-dAb. This observation is due to the scattering and absorption of MNPs aggregates that are pulled to the surface by the magnetic field gradient ∇B = 0.10 T mm^{-1}. After switching off the magnetic field (∇B = 0 T mm^{-1}) and rinsing the sensor surface with a buffer, a fast increase of reflectivity signal R is observed due to the release of MNP-dAb conjugates that were not bound to the captured *E. coli* O157:H7. For the sample spiked with *E. coli* O157:H7 at a concentration of 10^6 cfu mL^{-1}, the reflectivity change of ΔR = 0.12 was determined, which is 2 orders of magnitude higher than that measured by direct GC-SP resonance detection format. Let us note that this signal enhancement originates from combined effects of the MNP-enhanced mass transfer of the analyte to the surface (more than an order of magnitude higher rate is estimated based on the theory presented in the Supporting Information), increased refractive index changes associated with the analyte affinity binding to the sensor surface, and higher sensitivity of the GC-LRSP platform. Figure 5b also demonstrates that the target analyte captured by cAb on a surface can be fully released by the regeneration with NaOH allowing for multiple detection cycles on a single sensor chip.

The *E. coli* O157:H7 biosensor calibration curves were measured for each detection format in triplicate, and error bars were determined as the standard deviation. The limit of detection (LOD) was obtained as the concentration of *E. coli* O157:H7 in a sample for which the response ΔR reached 3 times the standard deviation ($3\sigma_R$) of the reflectivity baseline R. From results presented in Figure 6a, the LOD of 6.5 × 10^5 cfu mL^{-1} was estimated for the GC-SP sensor chip with direct measurement of *E. coli* O157:H7 binding-induced refractive index changes. The same figure shows that the implementation of the MNP-enhanced assay allowed decreasing the LOD by a factor of 650 to 10^3 cfu mL^{-1} on the GC-SP sensor chip. As seen in Figure 6b, the LOD was further improved to around 50 cfu mL^{-1} by using the same assay and the readout based on GC-LRSP, which corresponds to an enhancement by 4 orders of magnitude with respect to that observed for GC-SP and direct detection format. A control experiment in which a different but closely related bacterium (*E. coli* K12) was detected reveals excellent specificity of the developed biosensor, see Figure 6b. In general, the improvements in LOD are better than the enhancement of the sensor response ΔR observed for the binding of target analyte at concentration of 10^6 cfu mL^{-1} and from refractometric measurements. This may be ascribed to the nonlinear dependence of the sensor response ΔR on the concentration of the target analytes for two key reasons. First, we assume that the amount of MNP-dAb bound to target analyte is increasing when decreasing the concentration of *E. coli* O157:H7, which is associated with its more efficient delivery to the surface. This leads to larger enhancement of the sensor response at lower analyte concentrations and further improved the LOD. Second, the binding of MNPs to the surface is accompanied with scattering, effective refractive index change, and an increase in absorption. These multiple effects alter both the resonance angle and shape of the resonance dip which results in nonlinear dependence of the reflectivity change ΔR on the amount of MNP adhered to the surface. As compared to other techniques such as polymerase chain reaction (PCR, LOD = 6−10 cells),[25,26] enzyme linked immunosorbent assays (ELISA, LOD 10^3−10^5 cfu mL^{-1}),[27] quartz crystal microbalance (QCM, 10^3 cfu mL^{-1}),[28] and surface-enhanced Raman spectroscopy (SERS, LOD 5 cfu mL^{-1}, 10^6 cells mL^{-1}),[29,30] the reported method shows superior or similar sensitivity with shorter analysis time (30 min including incubation), which otherwise requires several hours or days.

CONCLUSIONS

A novel approach to SPR biosensors based on grating-coupled long-range surface plasmons (GC-LRSPs) advanced by MNP immunoassays was reported and applied for the detection of bacterial pathogen *E. coli* O157:H7. The sensor chip for accurate measurements of refractive index variations was developed by using nanoimprint lithography, and it provided about a 8.5-fold better refractive index resolution compared to regular grating-coupled surface plasmons (GC-SPs). With

dx.doi.org/10.1021/ac301904x | *Anal. Chem.* 2012, 84, 8345−8350

respect to the direct detection format, the MNP-enhanced assay provided additional enhancement of the sensor signal through a more efficient collecting of target analyte on the sensor surface and by the amplified refractive index contrast of the analyte. The assay based on GC-LRSP allowed for the detection of a target analyte, *E. coli* O157:H7, with the limit of detection of 50 cfu mL^{-1}, which was about 4 orders of magnitude better than that provided by regular GC-SP resonance with direct detection format.

■ ASSOCIATED CONTENT

Supporting Information

FEM simulation of the angular spectra for GC-LSP, refractometric experiments, and theoretical analysis of the diffusion rate and the MNPs velocity. This material is available free of charge via the Internet at http://pubs.acs.org.

■ AUTHOR INFORMATION

Corresponding Author

*Fax: +43(0)50550-4450. E-mail: jakub.dostalek@ait.ac.at.

Notes

The authors declare no competing financial interest.

■ ACKNOWLEDGMENTS

The authors would like to thank Marlies Czetina and Angela Sessitsch (AIT, Vienna) for the preparation of the *E. coli* K12 samples. In addition, we are grateful to Prof. Bernhard Schuster and Angelika Schrems (Department of Nanobiotechnology, University of Natural Resources and Life Sciences, Vienna) for the DLS measurements. The authors would like to acknowledge the partial support for this work provided by the Austrian NANO Initiative (FFG and BMVIT) through the NILPlasmonics Project within the NILAustria Cluster (www.NILAustria.at) and the Austrian Science Fund (FWF) through the Project ACTIPLAS (Grant P 244920-N20).

■ REFERENCES

(1) Homola, J. *Chem. Rev.* **2008**, *108*, 462−493.
(2) Subramanian, A.; Irudayaraj, J.; Ryan, T. *Biosens. Bioelectron.* **2006**, *21*, 998−1006.
(3) Taylor, A. D.; Ladd, J.; Yu, Q. M.; Chen, S. F.; Homola, J.; Jiang, S. Y. *Biosens. Bioelectron.* **2006**, *22*, 752−758.
(4) Koubová, V.; Brynda, E.; Karasová, L.; Škvor, J.; Homola, J; Dostálek, J.; Tobiška, P.; Rošický, J. *Sens. Actuators, B* **2001**, *74*, 100−105.
(5) Yanik, A. A.; Huang, M.; Kamohara, O.; Artar, A.; Geisbert, T. W.; Connor, J. H.; Altug, H. *Nano Lett.* **2010**, *10*, 4962−4969.
(6) Fang, S. P.; Lee, H. J.; Wark, A. W.; Corn, R. M. *J. Am. Chem. Soc.* **2006**, *128*, 14044−14046.
(7) He, L.; Musick, M. D.; Nicewarner, S. R.; Salinas, F. G.; Benkovic, S. J.; Natan, M. J.; Keating, C. D. *J. Am. Chem. Soc.* **2000**, *122*, 9071−9077.
(8) Wark, A. W.; Lee, H. J.; Qavi, A. J.; Corn, R. M. *Anal. Chem.* **2007**, *79*, 6697−6701.
(9) Mitchell, J. S.; Wu, Y. Q.; Cook, C. J.; Main, L. *Anal. Biochem.* **2005**, *343*, 125−135.
(10) Teramura, Y.; Arima, Y.; Iwata, H. *Anal. Biochem.* **2006**, *357*, 208−215.
(11) Tseng, P.; Di Carlo, D.; Judy, J. W. *Nano Lett.* **2009**, *9*, 3053−3059.
(12) Wang, J. L.; Munir, A.; Zhu, Z. Z.; Zhou, H. S. *Anal. Chem.* **2010**, *82*, 6782−6789.
(13) Wang, Y.; Dostalek, J.; Knoll, W. *Anal. Chem.* **2011**, *83*, 6202−6207.
(14) Soelberg, S. D.; Stevens, R. C.; Limaye, A. P.; Furlong, C. E. *Anal. Chem.* **2009**, *81*, 2357−2363.
(15) Dostalek, J.; Knoll, W. *Biointerphases* **2008**, *3*, 12−21.
(16) Stewart, M. E.; Anderton, C. R.; Thompson, L. B.; Maria, J.; Gray, S. K.; Rogers, J. A.; Nuzzo, R. G. *Chem. Rev.* **2008**, *108*, 494−521.
(17) Sepulveda, B.; Angelome, P. C.; Lechuga, L. M.; Liz-Marzan, L. M. *Nano Today* **2009**, *4*, 244−251.
(18) Sarid, D. *Phys. Rev. Lett.* **1981**, *47*, 1927−1930.
(19) Nenninger, G. G.; Tobiska, P.; Homola, J.; Yee, S. S. *Sens. Actuators, B* **2001**, *74*, 145−151.
(20) Dostalek, J.; Kasry, A.; Knoll, W. *Plasmonics* **2007**, *2*, 97−106.
(21) Vala, M.; Etheridge, S.; Roach, J. A.; Homola, J. *Sens. Actuators, B* **2009**, *139*, 59−63.
(22) Huang, C. J.; Sessitsch, A.; Dostalek, J.; Knoll, W. *Anal. Chem.* **2011**, *83*, 674−677.
(23) Cheng, L. J.; Kao, M. T.; Meyhofer, E.; Guo, L. J. *Small* **2005**, *1*, 409−414.
(24) Koh, I.; Wang, X.; Varughese, B.; Isaacs, L.; Ehrman, S. H.; English, D. S. *J. Phys. Chem. B* **2006**, *110*, 1553−1558.
(25) Belgrader, P.; Benett, W.; Hadley, D.; Richards, J.; Stratton, P.; Mariella, R.; Milanovich, F. *Science* **1999**, *284*, 449−450.
(26) Dharmasiri, U.; Witek, M. A.; Adams, A. A.; Osiri, J. K.; Hupert, M. L.; Bianchi, T. S.; Roelke, D. L.; Soper, S. A. *Anal. Chem.* **2010**, *82*, 2844−2849.
(27) Blais, B. W.; Leggate, J.; Bosley, J.; Martinez-Perez, A. *Lett. Appl. Microbiol.* **2004**, *39*, 516−522.
(28) Varshney, M; Li, Y. B. *Biosens. Bioelectron.* **2007**, *22*, 2408−2414.
(29) Knauer, M.; Ivleva, N. P.; Liu, X. J.; Niessner, R.; Haisch, C. *Anal. Chem.* **2010**, *82*, 2766−2772.
(30) Temur, E.; Boyaci, I. H.; Tamer, U.; Unsal, H.; Aydogan, N. *Anal. Bioanal. Chem.* **2010**, *397*, 1595−1604.